European Journal of Medicinal Chemistry 46 (2011) 1749–1756

Contents lists available at ScienceDirect

European Journal of Medicinal Chemistry

journal homepage: http://www.elsevier.com/locate/ejmech

Original article

Synthesis, biological evaluation and molecular modeling studies of quinolonyl diketo acid derivatives: New structural insight into the HIV-1 integrase inhibition

Pierre Vandurm [a,*,1], Allan Guiguen [b,1], Christine Cauvin [a], Benoît Georges [a], Kiet Le Van [a], Catherine Michaux [a], Christelle Cardona [b], Gladys Mbemba [c], Jean-François Mouscadet [c], László Hevesi [a,1], Carine Van Lint [b,**,1], Johan Wouters [a,***,1]

[a] Département de Chimie, Facultés Universitaires Notre-Dame de la Paix (FUNDP), B-Namur 5000, Belgium
[b] Laboratoire de Virologie Moléculaire, Institut de Biologie et de Médecine Moléculaires, Université Libre de Bruxelles (ULB), Gosselies B-6041, Belgium
[c] LBPA, CNRS, Ecole Normale Supérieure de Cachan, Cachan F-94235, France

ARTICLE INFO

Article history:
Received 25 November 2010
Received in revised form
10 February 2011
Accepted 13 February 2011
Available online 22 February 2011

Keywords:
Quinolonyl diketo acid
Antiviral activity
HIV-1 IN
Anti-integrase activity
Molecular modeling
Docking

ABSTRACT

New quinolonyl diketo acid compounds bearing various substituents at position 6 of the quinolone scaffold were designed and synthesized as potential HIV-1 integrase inhibitors. These new compounds were evaluated for their antiviral and anti-integrase activity and showed inhibitory potency similar to that of 6-bromide analog **2**. Molecular modeling and docking studies were performed to rationalize these data and to provide a detailed understanding of the mechanism of inhibition for this class of compounds.

1. Introduction

Integration of viral DNA into the host-cell chromosome is an obligatory step in the human immunodeficiency virus (HIV) replication cycle [1]. This process is catalyzed by the virally encoded integrase (IN) through two sequential reactions [2,3]. The first one, named 3′-processing (3′-P), corresponds to an endonucleolytic cleavage at each 3′ ends of double-stranded viral DNA extremities. The second step, strand transfer (ST), inserts the viral DNA into the host-cell DNA through a transesterification mechanism. HIV-1 IN belongs to a large family of polynucleotidyl transferase enzymes that include transposases, polymerases and other retroviral integrases [4–6]. The catalytic core domain (CCD) contains a conserved DDE motif which consists of two aspartates (D64 and D116) and one glutamate (E152), essential for enzymatic activity [7]. Crystal structures of the isolated CCDs available to date [8,9] show a single Mg^{2+} ion coordinated by the two aspartate residues (D64 and D116). Nevertheless, similar to other polynucleotidyl transferases, a second metal can be most likely coordinated by E152 (with D64) once HIV-1 IN binds to its DNA substrate [6]. Inhibitors of IN appear to be particularly promising since, unlike protease and reverse transcriptase, this enzyme does not have direct human homologs [10,11]. Among all reported IN inhibitors [12–14], the β-diketo acid (DKA) class of compounds has emerged as the most potent and the most promising. Raltegravir is the first approved IN inhibitor whereas Elvitegravir and GSK364735 have reached clinical development (Fig. 1) [15–19]. Like other well-known DKA inhibitors, these one share two common structural chemotypes essential for the anti-IN activity: a diketo acid chain able to interact with Mg^{2+} metal ions (marked in bold) and a properly oriented hydrophobic benzyl moiety (marked in dashed box). They selectively inhibit ST reaction, suggesting that they bind at the IN/DNA interface, acting as “interfacial inhibitors” [20,21]. Despite the lack of detailed structural information about HIV-1 IN/DNA interactions, this speculative mechanism of action tends to be validated by the recent X-ray crystal structure of IN from the prototype foamy virus (PFV-1 IN) in complex with its cognate viral DNA and ST inhibitors [22,23].

* Corresponding author. Tel.: +32 81 72 45 69.
** Corresponding author. Tel.: +32 2 650 98 07; fax: +32 2 650 98 00.
*** Corresponding author. Tel.: +32 81 72 45 50; fax: +32 81 72 54 40.
E-mail addresses: pierre.vandurm@fundp.ac.be (P. Vandurm), cvlint@ulb.ac.be (C. Van Lint), johan.wouters@fundp.ac.be (J. Wouters).
[1] These authors equally contributed to this work.

0223-5234/$ – see front matter © 2011 Elsevier Masson SAS. All rights reserved.
doi:10.1016/j.ejmech.2011.02.028

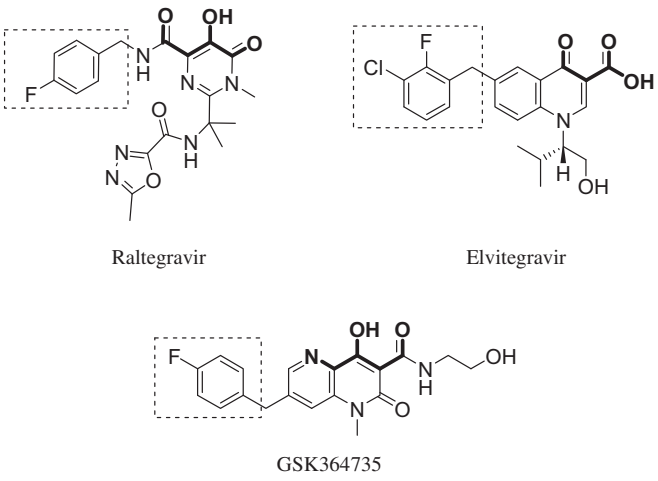

Fig. 1. Representative integrase strand transfer inhibitors (INSTIs). The two common structural chemotypes include a diketo acid moiety in bold and a hydrophobic benzyl moiety in dashed box.

Based on Di Santo's quinolone series, we have reported in a previous work [24] two compounds (compounds **1** and **2**, Fig. 2) as potential HIV-1 integrase inhibitors. Docking studies based on the HIV-1 IN CCD crystal structure [9] allowed to propose two binding modes for compound **2** pointing out the possibility to substitute the bromine atom at C-6. In order to gain new insights into the structural requirements for anti-IN activity as well as to elucidate the binding mode of this series of compounds, we here explored the effect of chemical modifications at position 6 of the quinolone scaffold. In this context, we synthesized new quinolone derivatives **3**–**6** (Fig. 2) by the replacement of bromine atom of **2** with bulky hydrophilic or hydrophobic substituents. All these compounds were evaluated for their anti-integrase and antiviral activity and structure–activity relationships were established. In addition, a new HIV-1 IN/DNA model was built considering two Mg^{2+} ions octahedrally coordinated. Docking studies were then performed to predict the binding mode of quinolone compounds and to rationalize the observed structure–activity relationships. Based on these results, a detailed mechanism of inhibition for quinolonyl DKA compounds is proposed.

2. Results and discussion

2.1. Chemistry

The title compounds **3**–**6** were synthesized according to Di Santo's procedure [25,26] with modifications as presented in Schemes 1 and 2. The key intermediate 3-acetyl-6-hydroxy-4(1*H*)-quinolinone **8** was obtained by reaction of commercially available 4-hydroxyaniline with ethylethoxymethyleneacetoacetate and subsequent thermal condensation in diphenyl ether. **8** was then N– and O–alkylated with 4-fluorobenzyl bromide in alkaline medium (K_2CO_3) to give compound **9**. The formation of N and O-benzyl derivative **9** was indicated by the presence of a singlet at 5,16 and 5,62 ppm for the N–CH_2 and O–CH_2. (*E*)-ethyl [3-acetyl-1-(4-fluorophenyl)methyl-4(1*H*)-quinolinon-6-yl]acrylate **11** was obtained by palladium-catalyzed Heck reaction of **10** (previously synthesized and described [24]) with acrylic acid ethyl ester. The presence of the *E* isomeric form was confirmed by ^{1}H NMR spectra, showing the appearance of two doublets at 6,51 and 7,73 ppm characteristic of α,β-unsaturated olefinic protons, with coupling constant 16 Hz. The diketo ester derivatives **3** and **5** were obtained by Claisen condensation of compounds **9** and **11**, respectively, with diethyl oxalate in the presence of sodium ethoxide. These compounds were in turn hydrolyzed by saponification reaction to give DKA derivatives **4** and **6**. Diketo ester/acid compounds were characterized by IR and ^{1}H NMR as well as by mass spectrometry. The presence of the keto-enolic ester/acid chain in synthesized compounds **3**–**6** was detected by the appearance of a strong singlet around 8 ppm characteristic of an enolic proton and three characteristic intense bands in the region around 1600–1750 cm^{-1} due to $\nu_{C=O}$ carboxylic acid, $\nu_{C=O}$ quinolone ring and coupled vibration band ($\nu_{C=O} + \nu_{C=C}$) of keto-enol group.

2.2. Biological evaluation

Diketo ester and acid derivatives **3**–**6** were tested *in vitro* for their ability to inhibit the 3′-P and the ST reaction in the presence of Mg^{2+} using a gel-based assay [27]. IC_{50} values were generated from duplicate experiments and calculated using dose response curves (Table 1). As already observed for quinolonyl DKA series [24–26], acidic derivatives were more potent than the corresponding esters, with a high selectivity against ST. The replacement of bromine atom at C-6 by an anionic (acrylate) or a hydrophobic (4-fluoro-benzyloxy) group does not lead to a significant improvement of HIV-1 IN inhibition. Compounds **4** and **6** showed IC_{50} values against ST (ST IC_{50} = 0.03–0.05 μM) similar to the one of 6-bromide analog **2** (ST IC_{50} = 0.03 μM) with a moderate increase in the selectivity for ST versus 3′-P. These results suggest that the size of substituents at C-6 on quinolone scaffold affect the ability of the inhibitor to discriminate between the active site of the DNA-bound or -unbound form of HIV-1 IN. Moreover, once the inhibitor is bound to the IN/DNA complex, substituents at C-6 do not make significant interaction.

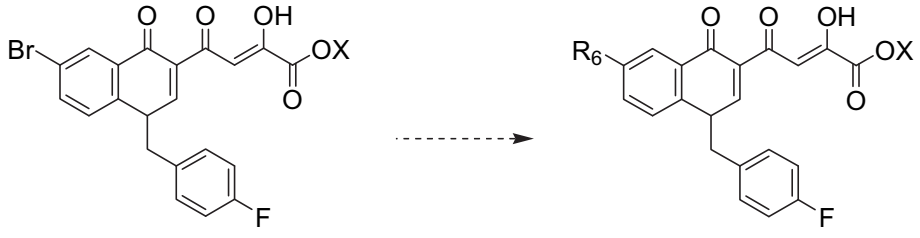

1: X = Et
2: X = H

3: X= Et; R_6 = O-CH_2(4-F-Ph)
4: X= H; R_6 = O-CH_2(4-F-Ph)
5: X= Et; R_6 = HC=CHCOOEt
6: X=H; R_6 = HC=CHCOOH

Fig. 2. Structure of 6-substituted quinolone compounds. Bromine atom of **2** was substituted by acrylic ester/acid and 4-fluoro-benzyloxy to generate new inhibitors **3**–**6**.

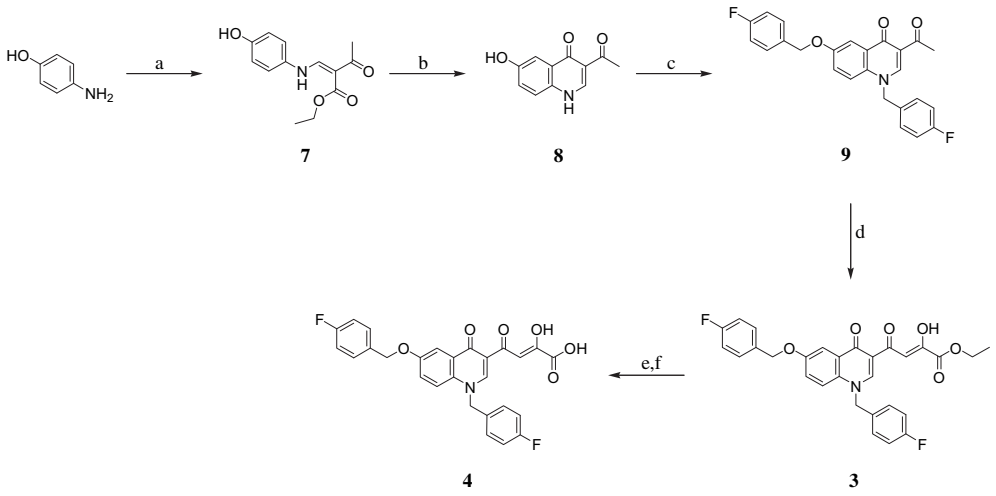

Scheme 1. Reagents and conditions: (a) ethylethoxymethyleneacetoacetate, 120 °C, 10 min; (b) Ph_2O, reflux 1.30 h; (c) 4-Fluorobenzyl bromide, K_2CO_3, DMF, 100 °C, 5 h; (d) diethyl oxalate, C_2H_5ONa, THF, 20 h, HCl, rt; (e) 1 N NaOH, THF/MeOH (1:1), 3 h; (f) HCl 1 N, rt.

The activity of the title quinolone compounds against wild-type HIV-1 was also established by determining their ability to inhibit viral infection of TZM-bl cells, as described elsewhere [28]. Cytotoxicity (CC_{50}) and antiviral activities (EC_{50}) of compounds **3**–**6** are presented in Table 1. All tested compounds showed antiviral activity at non-cytotoxic concentrations. All derivatives were characterized by low cytotoxicity with CC_{50} values up to 1 mM. The antiviral activities are correlated with the anti-integrase activities. Indeed, acidic derivatives **4** and **6** were more potent than the corresponding esters **3**,**5** and showed EC_{50} values similar to that of compound **2**.

2.3. Molecular modeling studies

2.3.1. HIV-1 IN/DNA complex building

Due to the lack of HIV-1 IN/DNA experimental structures, the building of a reliable model is essential for predicting docking of INSTIs. Based on the recent crystal structure of full-length foamy virus IN in complex with its cognate DNA and INSTIs, models of HIV-1 IN/DNA complex in its active and INSTI-inhibited forms have been reported [29,30]. Nevertheless, they did not consider the octahedral inner sphere coordination environments of the two active-site Mg^{2+} ions, in particular explicit water molecules which could be involved in the catalytic reaction mechanism. Interestingly, by superimposing the Cα atoms of the Tn5 transposase (PDB code 1MUS) [31], PFV IN (PDB code 3L2S) [22] and HIV-1 IN CCD (PDB code 1BL3C) [9] DDE active-site residues, water molecules present in both Tn5 transposase and HIV-1 IN crystal structures occupy similar positions and complete the octahedral geometry of the two divalent metal ions from PFV crystal structure (Fig. 3a). The 5′ phosphate group of Tn5 transposon superimposes with both bridging (w_4) and apical (w_1) water molecules from HIV-1 IN CCD. This superimposition reveals a plausible conformation of a scissile phosphodiester group from the target DNA interacting with the two divalent ions by displacing two water molecules. In this way, the scissile phosphodiester group might be properly positioned for the attack of the 3′-OH nucleophilic group of the viral DNA. These observations prompted us to build a model of the HIV-1 IN/DNA complex in its INSTI-inhibited form by

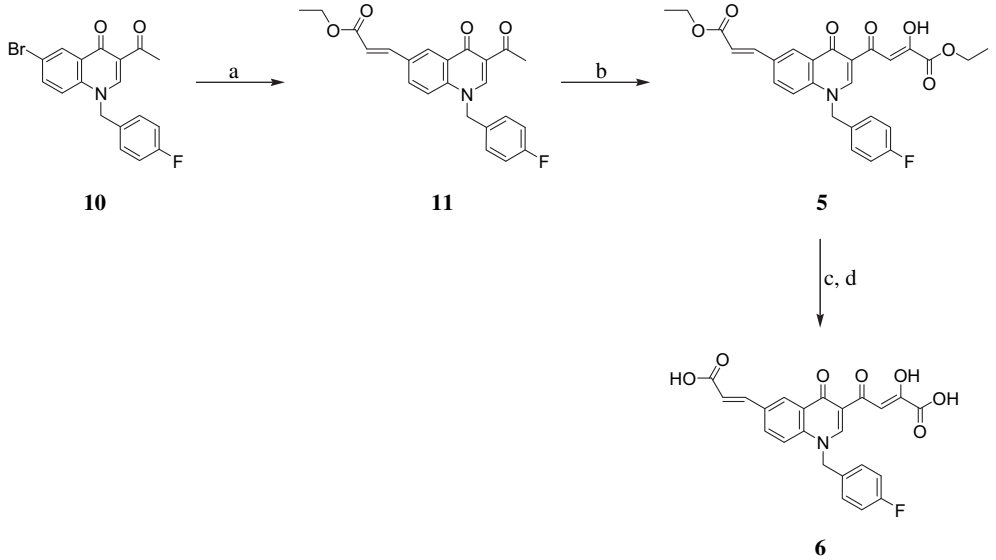

Scheme 2. Reagents and conditions: (a) $Pd(OAc)_2$ cat., PPh_3, NEt_3, acrylic acid ethyl ester, DMF, 80 °C, 48 h; (b) diethyl oxalate, C_2H_5ONa, THF, 20 h, HCl, rt; (c) 1 N NaOH, THF/MeOH (1:1), 3 h; (d) HCl 1 N, rt.

Table 1
Cytotoxicity, antiviral and anti-integrase activities of derivatives **3**–**6**.

Compd	R	X	anti-IN activity, IC_{50}[a]		antiviral activity		
			3′-P	ST	EC_{50}[b]	CC_{50}[c]	SI[d]
3	O–CH_2–4–F–Ph	Et	>300	>300	13	>1000	77
4	O–CH_2–4–F–Ph	H	3	0.05	1	>1000	1000
5	HC = CHCOOEt	Et	>300	>300	>140	>1000	7
6	HC = CHCOOH	H	8	0.03	5	>1000	200
2[e]	Br	H	1.6	0.03	4	>1000	250

[a] Inhibitory concentration 50% (μM) determined from dose response curves.
[b] *Ex vivo* anti-HIV activity (μM) (TZM-bl cell line [26]).
[c] Cytotoxic concentration 50% (μM) (TZM-bl cells).
[d] Selectivity index = CC_{50}/EC_{50}.
[e] Literature data: see ref [23].

superimposing the Cα atoms of HIV-1 IN CCD (PDB code 1BL3C) onto those of the Elvitegravir-bound PFV crystal structure (PDB code 3L2U) [22] and by considering explicit water molecules (see experimental section for details). This new model was subsequently optimized by a minimization procedure and used as template to perform docking studies.

2.3.2. Docking studies

Docking of the best DKA quinolone compounds (**2**, **4** and **6**) in the newly built model was performed with the Gold Software [32]. All these compounds showed a similar interfacial-binding mode in which the DKA moiety chelates the two Mg^{2+} ions (see docking result of **2**, Fig. 3b). In this orientation, the w_1 (bridging) and w_4 (apical) coordinated water molecules were totally displaced by carboxylate and enolate oxygen atoms, respectively, whereas the keto oxygen atom replaces the 3′-OH extremity of viral DNA. As a result, the displaced 3′-adenosine terminal base (A17) was involved in a π-stacking interaction with the quinolone ring in such a way that bromine atom at C-6 pointed out to the solvent-exposed surface. The *p*-F-benzyl group fitted within a tight pocket formed by cytosine 16 (C16), guanine 4 (G4) and two catalytic loop residues P145 and Q146. Fluorobenzyl group made π-stacking interaction with C16 taking the space originally occupied by A17. These docking results were in agreement with the structure–activity relationships that we observed above (see Section 2.2). Indeed, the chelation of the carboxylate group to Mg^{2+} ion could explain the stronger inhibitory potency of acidic compounds compared to ester compounds. Moreover, the orientation of the substituent at position 6 of the quinolone scaffold towards the solvent-exposed surface could also explain the unmodified potency of 6-substituted quinolone derivatives.

These molecular modeling studies allow us to propose a mechanism of inhibition by DKA compounds (Fig. 4). After the processing of viral DNA, the active site of HIV-1 IN adopts an active conformation in which two Mg^{2+} ions are octahedrally coordinated by the DDE motif, the 3′-OH extremity and water molecules. This active conformation facilitates the binding of a scissile phosphodiester group from target DNA which displaces bridging (w_1) and apical (w_4) water molecules from the active site, forming the ST complex. Once the inhibitor binds in the active site, the chelating moiety (DKA chain) interacts with the two Mg^{2+} ions by displacing the 3′-OH extremity and the two water molecules originally occupied by the phosphodiester group. The newly formed octahedral complex is then stabilized by the properly oriented hydrophobic benzyl moiety by replacing the 3′ A17 displaced from the active site to form a tighter complex. In this way, the inhibitor prevents the formation of the ST complex rendering it catalytically inactive. This mechanism of action is in agreement with the two-step mechanism of binding of INSTIs proposed by Garvey et al. [33].

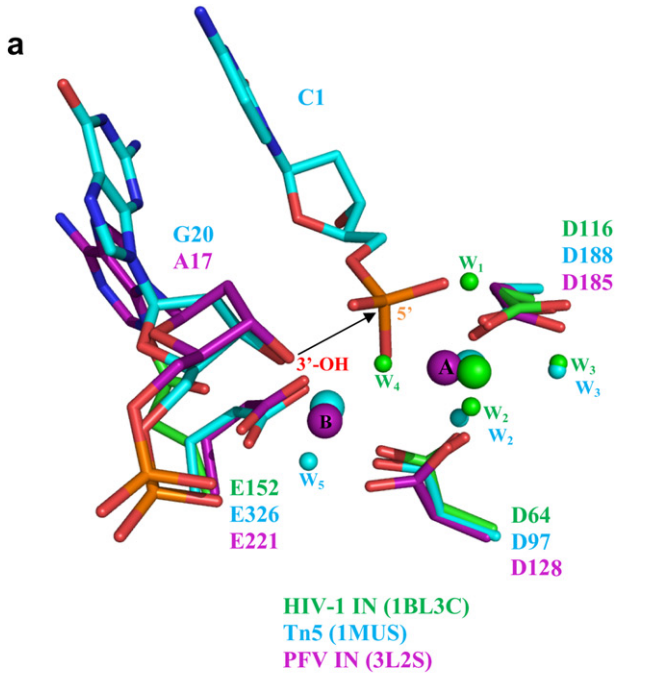

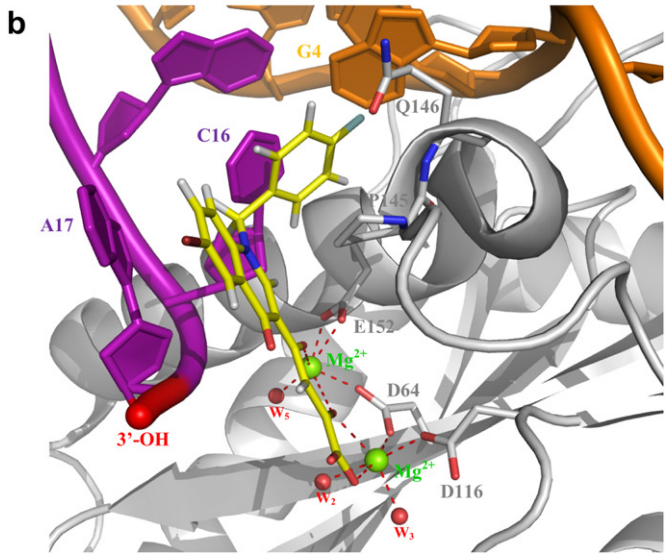

Fig. 3. a) Superimposition of the active sites of HIV-1 IN, Tn5 transposase and PFV IN based on the positions of C-α atoms of the active-site DDE residues. Side chains of DDE motif and terminal nucleotides are shown as sticks. Divalent metal ions (labeled A and B) and waters molecules (labeled w) are shown as spheres. The arrow indicates the 3′-OH end attacking the scissile phosphate of the target DNA mimicked by the 5′-phosphate end of Tn5 transposon. b) Docking result of compound **2** (yellow) into the HIV-1 IN/DNA model. The two Mg^{2+} ions and coordinated water molecules (w) are shown as green and red spheres, respectively. The nontransferred (orange) and reactive (magenta) DNA strand are shown as cartoon. Catalytic core domain is shown as grey cartoon with main amino acids as sticks. Note that the two Mg^{2+} ions are octahedrally coordinated to DDE motif, water molecules and the diketo acid chain of the quinolone inhibitor. (For interpretation of the references to colour in this figure legend, the reader is referred to the web version of this article.)

3. Conclusion

In order to elucidate the binding mode of DKA quinolonyl series of compounds, new derivatives were synthesized by replacing the 6-bromo atom of compound **2** by an acrylate and a p-fluoro-benzyloxy group. These compounds were evaluated for their enzymatic

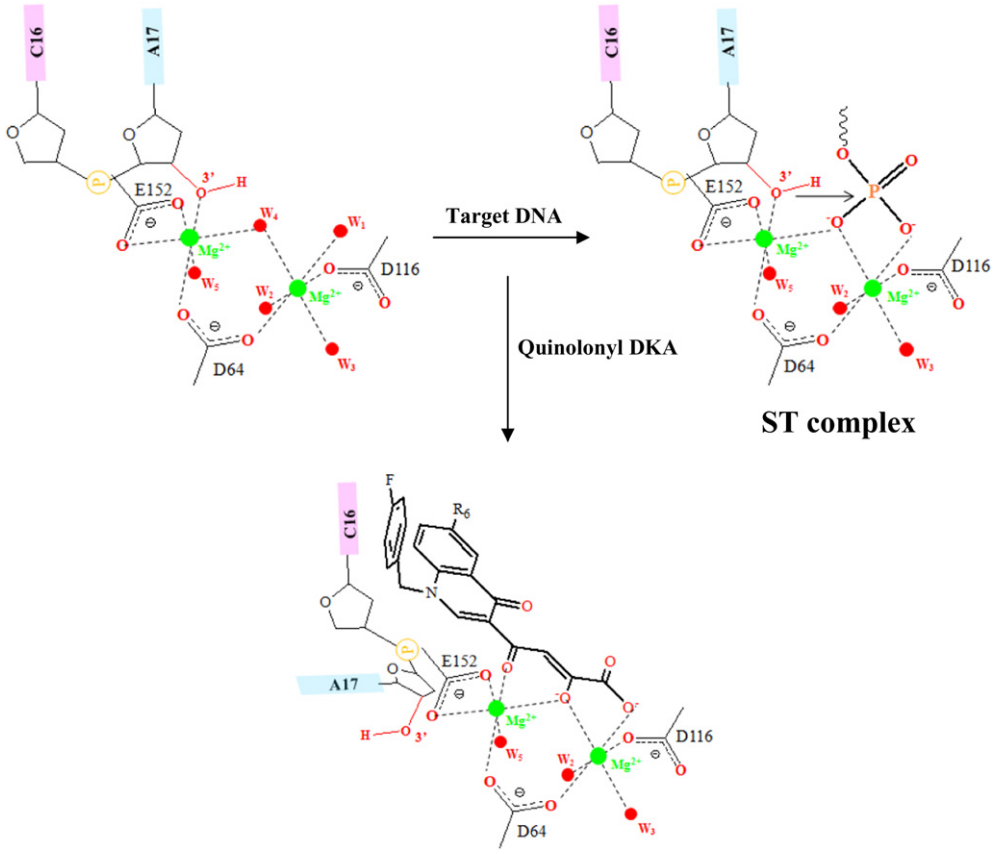

Fig. 4. Mechanism of inhibition for quinolonyl DKA compounds.

and antiviral activity. The introduction of both hydrophilic and hydrophobic substituents at C-6 did not have any effect on the activity in comparison with the activity observed with compound **2**. Structural analysis of the catalytic core domain of HIV-1 IN, Tn5 transposase and PFV IN led us to build a new HIV-1 IN/DNA model taking into account explicit water molecules to complete the octahedral geometry of the two active-site magnesium ions. Our further docking studies including water molecules predicted a binding mode in agreement with the biological activities we observed. Molecular modeling studies allowed to propose a detailed mechanism of inhibition for quinolonyl DKA compounds. We provided new structural insight into the mechanism of action of INSTIs which could be useful for the design of new HIV-1 IN inhibitors.

4. Experimental

4.1. Chemistry

All the reagents and solvents employed were used without further purification. ^{1}H NMR and and ^{13}C NMR spectra were recorded on a Jeol JNM EX-400 spectrometer. Chemical shifts (δ scale) are reported in parts per million (ppm) downfield from tetramethylsilane (TMS) used as an internal standard. Infrared (IR) spectra were recorded to the solid state on a Perkin–Elmer Spectrum 65. Melting points were determined with a TOTOLLI-BUCHI Melting Point B-545 apparatus. Analytical thin-layer chromatography (TLC) was done on Merck silica gel 60 F_{254} plates. Mass spectra were recorded on an 1100 series MSD Trap spectrometer equipped with an electron spray ionization (ESI) source.

4.1.1. Synthesis of 2-[[(4-phenol)amino]methylene]-3-oxobutanoic acid ethyl ester (**7**)

An equimolar mixture of ethylethoxymethyleneacetoacetate (4.6 g, 23 mmol) and 4-hydroxyaniline (2.5 g, 23 mmol) was stirred at 120 °C for 10 min. After cooling, the formed precipitate was filtered and washed with *n*-hexane to obtain pure compound **7** used in the next reaction without further purification. Yellow solid, yield: 55%, mp: 113 °C. ^{1}H NMR (DMSO-d_6, 400 MHz): δ 1.22 (t, 3H, CH_2CH_3), 2.36 (s, 3H, CH_3), 2.54 (s, 3H, CH_3), 4.10 (q, 2H, CH_2CH_3), 6.76 (d, 2H, J = 8.8 Hz, benzene H), 7.18 (d, 2H, J = 8.8 Hz, benzene H), 8.29 (d, 1H, J = 13.7 Hz, C=CH), 9.54 (s, 1H, OH), 12.54 (d, 1H, J = 13.7 Hz, NH).

4.1.2. Synthesis of 3-acetyl-6-hydroxy-4(1H)-quinolinone (**8**)

4.2 g (17 mmol) was added portion wise to 200 ml of boiling diphenyl ether previously heated at 250 °C. The solution was kept at 250 °C for 1 h and 30 min. After cooling, the formed precipitate was collected. The crude product was purified by chromatography on silica gel column (EtOH/CH_2Cl_2 as eluant) to provide pure derivative **8**. Brown solid, yield: 46%, mp: >250 °C. ^{1}H NMR (DMSO-d_6, 400 MHz): δ 2.56 (s, 1H, CH_3), 7.15 (dd, 1H, $J_{7,5}$ = 2.6 Hz, $J_{7,8}$ = 8.7 Hz, C_7-H quinolinone), 7.46 (d, 1H, $J_{8,7}$ = 8.7 Hz, C_8-H quinolinone), 7.51 (d, 1H, $J_{5,7}$ = 2.6 Hz, C_5-H quinolinone), 8.37 (s, 1H, C_2-H quinolinone), 9.91 (bs, 1H, OH).

4.1.3. Synthesis of 3-acetyl-1-((4-fluorophenyl)methyl)-6-(4-fluorobenzyloxy)-4(1H) quinolinone (**9**)

4-Fluorophenylmethyl bromide (1.7 g, 9 mmol) and anhydrous K_2CO_3 (1.3 g, 9 mmol) was added to a mixture of **8** in dry DMF (30 ml). The resulting suspension was stirred at 100 °C for 5 h. After the mixture was cooled, water (50 ml) was added and the

precipitate was filtered, washed with petroleum ether and purified by chromatography on silica gel column (AcOEt/petroleum ether 4/6 and then AcOEt as eluant). Yellow solid, yield: 73%, mp: 219 °C. ^{1}H NMR (DMSO-d_6, 400 MHz): δ 2.61 (s, 3H, CH_3), 5.16 (s, 2H, CH_2), 5.62 (s, 2H, CH_2), 7.1–7.3 (m, 6H, Ar–H), 7.35 (dd, 1H, $J_{7,5}$ = 3 Hz, $J_{7,8}$ = 9.4 Hz, C_7-H quinolinone), 7.44–7.52 (m, 2H, Ar–H), 7.61 (d, 1H, $J_{8,7}$ = 9.4 Hz, C_8-H quinolinone), 8.65 (d, 1H, $J_{5,7}$ = 3 Hz, C_5-H quinolinone), 8.78 (s, 1H, C_2-H quinolinone).

*4.1.4. Synthesis of (E)-ethyl [3-acetyl-1-(4-fluorophenyl)methyl-4 (1H)-quinolinon-6-yl] acrylate (**11**)*

3-acetyl-6-bromo-1-((4-fluorophenyl)methyl)-4(*1H*)-quinolinone (**10**) (0.450 g, 1.2 mmol) was added to a mixture of acrylic acid ethyl ester (0.202 g, 2.4 mmol), $Pd(OAc)_2$ (0.013 g, 0.06 mmol), PPh_3 (0.061 g, 0.24 mmol) and NEt_3 (0.134 g, 1.2 mmol) in 3 ml of DMF. The reaction mixture was stirred under argon for 48 h at 80 °C. The reaction was cooled to room temperature and extracted with ethyl acetate. The organic phases were washed four times with brine (10 ml) and dried with $MgSO_4$. Upon removal of the solvent, the residue obtained was purified by chromatography on silica gel column (ACOEt/petroleum ether 3/7 and then 1/1 as eluant) to afford pure derivative **11**. Yellow solid, yield: 62%, mp: 220 °C. ^{1}H NMR ($CDCl_3$, 400 MHz): δ 1.33 (t, 3H, CH_2CH_3), 2.82 (s, 3H, CH_3), 4.26 (q, 2H, CH_3CH_2), 5.38 (s, 2H, CH_2), 6.51 (d, 1H, J_{trans} = 16 Hz, CH=CH), 7.02–7.18 (m, 4H, Ar–H), 7.32 (d, 1H, $J_{8,7}$ = 8.9 Hz, C_8-H quinolinone), 7.71 (dd, 1H, $J_{7,5}$ = 1 Hz, $J_{7,8}$ = 8.9 Hz, C_7-H quinolinone), 7.73 (d, 1H, J_{trans} = 16 Hz, CH=CH), 8.59 (s, 1H, C_2-H quinolinone), 8.65 (d, 1H, $J_{5,7}$ = 1 Hz, C_5-H quinolinone).

*4.1.5. General synthesis procedure for diketo esters (**3** and **5**)*

Freshly prepared sodium ethoxide (0.272 g, 2 mmol) was added to a well stirred mixture of diethyl oxalate (0.584 g, 4 mmol) and appropriate acetyl derivative **9** or **11** (2 mmol) in anhydrous THF (2 ml) under nitrogen atmosphere. The reaction mixture was stirred at room temperature for 20 h. *n*-hexane (70 ml) was added and the formed precipitate was filtered, washed with *n*-hexane and stirred for 30 min in 1N HCl (70 ml). The solid was filtered off and washed with *n*-hexane. Residual water was removed by azeotropic distillation using acetonitrile to provide pure diketo esters **3** and **5**.

*4.1.5.1. 4-[6-(4-fluorobenzyloxy)-1-(4-fluorophenyl)methyl-4(1H)-quinolinon-3-yl]-2-hydroxy-4-oxo-2-butenoic acid ethyl ester (**3**).* Yellow solid, yield: 82%, mp: 160 °C. IR υ_{max} (KBr/cm^{-1}): 1743 (C=O carboxylic acid), 1634 (C=O quinolinone), 1605 (C=O + C=C keto-enol). ^{1}H NMR (DMSO-d_6, 400 MHz): δ 1.28 (t, 3H, CH_2CH_3), 4.27 (q, 2H, CH_2CH_3), 5.17 (s, 2H, CH_2), 5.72 (s, 2H, CH_2), 7.09–7.34 (m, 6H, Ar–H), 7.39 (dd, 1H, $J_{7,5}$ = 3 Hz, $J_{7,8}$ = 9.4 Hz, C_7-H quinolinone), 7.43–7.53 (m, 2H, Ar–H), 7.66 (d, 1H, $J_{8,7}$ = 9.4 Hz, C_8-H quinolinone), 7.79 (d, 1H, $J_{5,7}$ = 3 Hz, C_5-H quinolinone), 8.00 (s, 1H, C_3-H butenoate), 9.04 (s, 1H, C_2-H quinolinone). ^{13}C NMR ($CDCl_3$, 400 MHz): 14.26 (CH_3), 57.59 (N–CH_2), 62.42 (CH_2), 69.91 (O–CH_2), 102.47 (CH), 108.58 (CH), 114.27 (C), 115.72 (d, J = 22.0 Hz, 2CH), 116.65 (d, J = 22.0 Hz, 2CH), 118.71 (CH), 123.68 (CH), 128.12 (d, J = 8.6 Hz, 2CH), 129.66 (d, J = 8.6 Hz, 2CH), 130.55 (C), 131.90 (d, J = 2.8 Hz, C), 133.28 (C), 147.50 (CH), 156.77 (C), 162.62 (C), 162.73 (d, J = 247.28 Hz, C), 162.81 (d, J = 248.24 Hz, C), 169.21 (C), 174.83 (C), 188.09 (C). LC-MS: $(M + H)^+$ 520.0.

*4.1.5.2. 4-[6-((E)-3-ethoxy-3-oxoprop-1-enyl)-1-(4-fluorophenyl)methyl-4(1H)-quinolinon-3-yl]-2-hydroxy-4-oxo-2-butenoic acid ethyl ester (**5**).* Yellow solid, yield: 79%, mp: 146 °C. IR υ_{max} (KBr/cm^{-1}): 1733 (C=O carboxylic acid), 1702 (C=O acrylic ester), 1644 (C=O quinolinone), 1600 (C=O + C=C keto-enol). ^{1}H NMR ($CDCl_3$, 400 MHz): δ 1.33 (t, 3H, CH_2CH_3), 1.41 (t, 3H, CH_2CH_3), 4.26 (q, 2H, CH_2CH_3), 4.40 (q, 2H, CH_2CH_3), 5.42 (s, 2H, CH_2), 6.52 (d, 1H, J_{trans} = 16 Hz, CH=CH), 7.04–7.20 (m, 4H, Ar–H), 7.36 (d, 1H, $J_{8,7}$ = 8.7 Hz, C_8-H quinolinone), 7.69–7.76 (m, 2H, CH=CH and C_7-H quinolinone), 8.11 (s, 1H, C_3-H butenoate), 8.67 (d, 1H, $J_{5,7}$ = 2 Hz, C_5-H quinolinone), 8.72 (s, 1H, C_2-H quinolinone). ^{13}C NMR ($CDCl_3$, 400 MHz): 14.24 (CH_3), 14.37 (CH_3), 57.46 (N–CH_2), 60.87 (CH_2), 62.51 (CH_2), 102.51 (CH), 115.80 (C), 116.78 (d, J = 22.0 Hz, 2CH), 117.54 (CH), 120.37 (CH), 127.93 (CH), 128.10 (d, J = 8.6 Hz, 2CH), 129.29 (C), 129.39 (d, J = 2.8 Hz, C), 131.86 (C), 132.23 (CH), 139.62 (C), 142.36 (CH), 148.68 (CH), 162.45 (C), 162.90 (d, J = 249.20 Hz, C), 166.58 (C), 169.58 (C), 174.96 (C), 187.55 (C). LC-MS: $(M + H)^+$ 494.0.

*4.1.6. General synthesis procedure for diketo acids (**4** and **6**)*

A mixture of the appropriate ester **3** or **5** (1.3 mmol) and 1N NaOH (12 ml) in THF/methanol (1:1, 15 ml) was stirred at room temperature for 3 h under nitrogen atmosphere, poured onto crushed ice and treated with 1N HCl to reach pH 2. The formed precipitate was filtered off and successively washed with water, ethanol and petroleum ether to give pure acids **4** and **6**.

*4.1.6.1. 4-[6-(4-fluorobenzyloxy)-1-(4-fluorophenyl)methyl-4(1H)-quinolinon-3-yl]-2-hydroxy-4-oxo-2-butenoic acid (**4**).* Yellow solid, yield: 79%, mp: 194 °C. IR υ_{max} (KBr/cm^{-1}): 1731 (C=O carboxylic acid), 1718 (C=O quinolinone), 1612 (C=O + C=C keto-enol). ^{1}H NMR (DMSO-d_6, 400 MHz): δ 5.17 (s, 2H, CH_2), 5.71 (s, 2H, CH_2), 7.09–7.34 (m, 6H, Ar–H), 7.39 (m, 1H, C_7-H quinolinone), 7.43–7.53 (m, 2H, Ar–H), 7.68 (d, 1H, $J_{8,7}$ = 9.4 Hz, C_8-H quinolinone), 7.77 (d, 1H, $J_{5,7}$ = 3 Hz, C_5-H quinolinone), 7.99 (s, 1H, C_3-H butenoate), 9.03 (s, 1H, C_2-H quinolinone). ^{13}C NMR (DMSO-d_6, 400 MHz): 56.13 (N–CH_2), 69.47 (O–CH_2), 102.10 (CH), 108.93 (CH), 113.35 (C), 115.86 (d, J = 22.0 Hz, 2CH), 116.32 (d, J = 21.0 Hz, 2CH), 120.64 (CH), 123.11 (CH), 129.39 (d, J = 7.6 Hz, 2CH), 130.31 (C), 130.57 (d, J = 8.6 Hz, 2CH), 132.35 (C), 133.30 (d, J = 1.9 Hz, C), 133.56 (C), 148.96 (CH), 156.61 (C), 162.22 (d, J = 244.41 Hz, C), 162.36 (d, J = 243.45 Hz, C), 164.22 (C), 174.33 (C). LC-MS: $(M + H)^+$ 492.0.

*4.1.6.2. 4-[6-((E)-3-hydroxy-3-oxoprop-1-enyl)-1-(4-fluorophenyl) methyl-4(1H)-quinolinon-3-yl]-2-hydroxy-4-oxo-2-butenoic acid (**6**).* Yellow solid, yield: 70%, mp: 163 °C. IR υ_{max} (KBr/cm^{-1}): 1703 (C=O carboxylic acid), 1698 (C=O acrylic acid), 1636 (C=O quinolinone), 1599 (C=O + C=C keto-enol). ^{1}H NMR (DMSO-d_6, 400 MHz): δ 5.75 (s, 2H, CH_2), 6.58 (d, 1H, J_{trans} = 16 Hz, CH=CH), 7.05–7.42 (m, 4H, Ar–H), 7.61–7.78 (m, 2H, CH=CH and C_8-H quinolinone), 7.96 (s, 1H, C_3-H butenoate), 8.05 (m, 1H, C_7-H quinolinone), 8.43 (d, 1H, $J_{5,7}$ = 2 Hz, C_5-H quinolinone), 9.08 (s, 1H, C_2-H quinolinone). ^{13}C NMR (DMSO-d_6, 400 MHz): 56.01 (N–CH_2), 102.17 (CH), 116.35 (d, J = 22.0 Hz, 2CH), 119.46 (CH), 121.19 (CH), 127.61 (CH), 129.41 (d, J = 8.6 Hz, 2CH), 132.06 (C), 132.28 (d, J = 1.9 Hz, C), 140.07 (C), 142.85 (CH), 150.01 (C), 150.42 (CH), 162.32 (d, J = 245.37 Hz, C), 162.85 (C), 164.19 (C), 167.87 (C), 174.65 (C). LC-MS: $(M + H)^+$ 438.0.

4.2. Biological assays

4.2.1. Cells and viruses

The following reagents were obtained through the AIDS Research and Reference Reagent Program, Division of AIDS, NIAID, NIH: TZM-bl from Dr. John C. Kappes, Dr. Xiaoyun Wu and Tranzyme Inc. TZM-bl cells were grown at 37 °C, 5% CO_2 in DMEM medium (Invitrogen) supplemented with 5% (v/v) heat-inactivated bovine serum, 50 U of penicilin/ml and 50 μg of streptomycin/ml (Invitrogen). Exponentially growing cells were trypsinised, centrifuged and split twice weekly. The HIV strain used in this study is HIV-1 NL4-3 derived from the infectious molecular clone pNL4-3. HIV-1 stocks were stored as cell-free supernatants at −80 °C.

4.2.2. In vitro assays

Compounds **3**–**6** were tested *in vitro* for 3′-P and ST inhibition in the presence of magnesium (Mg^{2+}) using a gel-based assay [27]. In this assay, the extent of 3′-P and ST was analyzed by using as substrate a 5′-^{32}P end-labeled 21-mer double-stranded DNA oligonucleotide corresponding to the last 21 bases of the U5 viral LTR. IN^{1-288} (400 nM) was incubated with 12.5 nM of the 5′-end ^{32}P-labeled oligonucleotide substrate in a reaction buffer (20 mM HEPES $pH_{7.5}$, 1 mM DTT, 10 mM $MgCl_2$, 10% dimethyl sulfoxyde) 1 h at 37 °C. Oligonucleotides were precipitated in a precipitation buffer (3M sodium acetate pH_7, 10 mg/ml glycogen, Tris-EDTA $pH_{7.5}$), extracted with phenol/chloroform and washed with ethanol. The oligonucleotides were resuspended in 10 μl of 10 mM formamide/EDTA, denatured and separated by electrophoresis on a polyacrylamide/urea gel (16% acrylamide, 7 M urea). Gels were dried, exposed in a PhosphorImager cassette, analyzed using a Storm mode imager (Amersham Biosciences) and quantified using ImageQuant. The IC_{50} values were determined from a curve (drug concentration versus percent inhibition) fitted on experimental data (Prism software) to obtain the concentration that produced 50% inhibition.

4.2.3. Antiviral activity

Antiviral activity of the compounds was evaluated using the TZM-bl [28] cell line. This TZM-bl cell line uses a Tat protein-induced transactivation of the HIV-1 LTR promoter driving the expression of the β-galactosidase gene. In brief, exponentially growing cells were plated at 5000 cells/well in flat-bottom 96-well microtiter plates. After a 48 h incubation, the medium was removed and replaced by 100 μl of medium containing the quinolinone derivatives at concentrations ranging from 0.00128 to 4 μM. Four hours after drug treatment, cells were infected with equal amount of cell-free virus (NL4-3 strain), corresponding to 100 ng of HIV p24 antigen. Forty-eight hours post-infection, the medium was removed and cells were lysed in PBS containing 0.1% NP-40 and 5 mM $MgCl_2$. β-galactosidase activity was measured using chlorophenol red β-D-galactopyranoside (Roche) assays. The 50% effective concentration (EC_{50}) was calculated from each dose response curve using Prism software.

4.2.4. Cytotoxicity

Flat-bottom 96-well plates were filled with 50 μl of complete medium containing 5000 TZM-bl cells. Two hours later, 50 μl of medium containing an appropriate dilution of the test compounds (from 100 to 0.032 μM) was added. Cells and compounds were incubated at 37 °C in growth medium for 3 days. Cell viability was determined by a colorimetric assay based on the cleavage of the tetrazolium salt WST-1 (Roche) by mitochondrial dehydrogenases in viable cells. Absorbance of converted dye was measured in an ELISA plate reader at the wavelength of 570 nm. The cytotoxicity of the compounds was calculated as the reduction percentage of viable cells observed in the drug-free control cell culture. The drug concentration required to reduce cell viability by 50% was named CC_{50}.

4.3. Molecular modeling

4.3.1. Model building

The HIV-1 IN/DNA model in its INSTI-inhibited form was initiated by overlaying the structures of HIV-1 IN CCD (1BL3C), Tn5 transposome (1MUS) and elvitegravir-bound PFV structure (3L2U) with their Cα positions of active-site residues Asp64, Asp116, and Glu152 (DDE motif). Bases of the 19-mer PFV DNA properly oriented into the HIV-1 IN CCD were mutated in order to correspond to the HIV-1 DNA sequence. Two Mg^{2+} ions were then modeled into the HIV-1 active site based on the two Mn^{2+} ions coordinates from PFV structure and glutamate 152 residue (E152) was reoriented to interact with Mg^{2+} ions. Coordinated water molecules present in both HIV-1 IN CCD and Tn5 transposome crystal structure were then merged into the HIV-1 model to complete the octahedral geometry of the two Mg^{2+} ions. The slightly resolved active-site loop (residues 141–148) was removed and replaced by the equivalent PFV IN loop (residues 210–217), after which residues were mutated to correspond to the HIV-1 IN sequence. To remove bad intramolecular contacts without altering the architecture of the binding site, the resulting model was energy-minimized by 500 steps of steepest descent using CHARMm force field and Generalized Born (GB) model as solvation treatment implemented in Discovery Studio 2.5 [34]. Coordinates of model are available upon request to the authors.

4.3.2. Docking

Docking of quinolone compounds into the HIV-1 IN/DNA model was carried out using GOLD (version 1.3.1) Software [30]. All compounds were modeled by considering the stable conformation previously identified by experimental and theoretical studies [35]. The binding region was defined as a 15 Å radius sphere centered on Mg^{2+} ions chelated by E152. An octahedral geometry was imposed on the two Mg^{2+} ions whereas explicit water molecules were allowed to switch on and off and to rotate around their three principal axes. For the 30 genetic algorithm (GA) runs performed, a total of 100 000 genetic operations were carried out on five islands, each containing 100 individuals. The niche size was set to 2, and the value for the selection pressure was set to 1.1. Genetic operator weights for crossover, mutation, and migration were set to 95, 95 and 10, respectively. The scoring function used to rank the docking was Goldscore. IN/DNA/ligand complex obtained by docking studies were minimized using steepest descent method (10 kcal mol^{-1} $Å^{-1}$ convergence) followed by conjugate gradient minimization (0.0001 kcal mol^{-1} $Å^{-1}$ convergence) imposing the coplanarity of the diketo acid moiety. All complexes were minimized using CHARMm force field and GB model as solvation treatment implemented in Discovery Studio 2.5 [34].

Acknowledgements

This research was supported in part by grants from the DGTRE (Direction générale des Technologies, de la Recherche et de l'Energie, Région Wallonne) (Programs WALEO 06/1/6295 and 05/1/5995). CVL is Directeur de Recherches of the Belgian "Fonds de la Recherche Scientifique-FNRS" (FRS-FNRS). P. Vandurm is a fellow of the FRIA/FNRS. A. Guiguen is a Postdoctoral fellow of the FRS-FNRS. C. Michaux is a Research Associate of the FRS-FNRS.

References

[1] E. Asante-Appiah, A.M. Skalka, Antivir. Res. 36 (1997) 139–156.
[2] T.K. Chiu, D.R. Davies, Curr. Top. Med. Chem. 4 (2004) 965–977.
[3] O. Delelis, K. Carayon, A. Sa, E. Deprez, J.-F. Mouscadet, Retrovirology 5 (2008) 114.
[4] P. Rice, R. Craigie, D.R. Davies, Curr. Opin. Struct. Biol. 6 (1996) 76–83.
[5] P.A. Rice, T.A. Baker, Nat. Struct. Biol. 8 (2001) 302–307.
[6] M. Nowotny, EMBO Reports 10 (2009) 144–151.
[7] D. Esposito, R. Craigie, Adv. Virus Res. 52 (1999) 319–333.
[8] Y. Goldgur, F. Dyda, A.B. Hickman, T.M. Jenkins, R. Craigie, D.R. Davies, Proc. Natl. Acad. Sci. USA 95 (1998) 9150–9154.
[9] S. Maignan, J.P. Guilloteau, Q. Zhou-Liu, C. Clement-Mella, V. Mikol, J. Mol. Biol. 282 (1998) 359–368.
[10] R.L. LaFemina, C.L. Schneider, H.L. Robbins, P.L. Callahan, K. LeGrow, E. Roth, W.A. Schleif, E.A. Emini, J. Virol. 66 (1992) 7414–7419.
[11] Z. Debyser, P. Cherepanov, B. Van Maele, E. De Clercq, M. Witvrouw, Antivir. Chem. Chemother. 13 (2002) 1–15.
[12] P. Cotelle, Recent Pat. Anti-Infect. Drug Discov. 1 (2006) 1–15.
[13] E. Serrao, S. Odde, K. Ramkumar, N. Neamati, Retrovirology 6 (2009) 25.
[14] D.J. McColl, X. Chen, Antivir. Res 85 (2010) 101–118.
[15] V. Summa, A. Petrocchi, F. Bonelli, B. Crescenzi, M. Donghi, M. Ferrara, F. Fiore, C. Gardelli, O. Gonzalez Paz, D.J. Hazuda, P. Jones, O. Kinzel, R. Laufer, E. Monteagudo, E. Muraglia, E. Nizi, F. Orvieto, P. Pace, G. Pescatore, R. Scarpelli, K. Stillmock, M.V. Witmer, M. Rowley, J. Med. Chem. 51 (2008) 5843–5855.

[16] M. Sato, T. Motomura, H. Aramaki, T. Matsuda, M. Yamashita, Y. Ito, H. Kawakami, Y. Matsuzaki, W. Watanabe, K. Yamataka, S. Ikeda, E. Kodama, M. Matsuoka, H. Shinkai, J. Med. Chem. 49 (2006) 1506–1508.
[17] M. Sato, H. Kawakami, T. Motomura, H. Aramaki, T. Matsuda, M. Yamashita, Y. Ito, Y. Matsuzaki, K. Yamataka, S. Ikeda, H. Shinkai, J. Med. Chem. 52 (2009) 4869–4882.
[18] D. Hazuda, M. Iwamoto, L. Wenning, Annu. Rev. Pharmacol. Toxicol. 49 (2009) 377–394.
[19] E.P. Garvey, B.A. Johns, M.J. Gartland, S.A. Foster, W.H. Miller, R.G. Ferris, R.J. Hazen, M.R. Underwood, E.E. Boros, J.B. Thompson, J.G. Weatherhead, C.S. Koble, S.H. Allen, L.T. Schaller, R.G. Sherrill, T. Yoshinaga, M. Kobayoshi, C. Wakasa-Morimoto, S. Miki, K. Nakahara, T. Noshi, A. Sato, T. Fujiwara, Antimicrob. Agents Chemother. 52 (2008) 901–908.
[20] A.S. Espeseth, P. Felock, A. Wolfe, M. Witmer, J. Grobler, N. Anthony, M. Egbertson, J.Y. Melamed, S. Young, T. Hamill, J.L. Cole, D.J. Hazuda, Proc. Natl. Acad. Sci. U.S.A. 97 (2000) 11244–11249.
[21] A. Bacchi, M. Biemmi, M. Carcelli, F. Carta, C. Compari, E. Fisicaro, D. Rogolino, M. Sechi, M. Sippel, C.A. Sotriffer, T.W. Sanchez, N. Neamati, J. Med. Chem. 51 (2008) 7253–7264.
[22] S. Hare, S.S. Gupta, E. Valkov, A. Engelman, P. Cherepanov, Nature 464 (2010) 232–236.
[23] S. Hare, A.M. Vos, R.F. Clayton, J.W. Thuring, M.D. Cummings, P. Cherepanov, Nature 107 (2010) 20057–20062.
[24] P. Vandurm, C. Cauvin, A. Guiguen, B. Georges, K. Le Van, V. Martinelli, C. Cardona, G. Mbemba, J.-F. Mouscadet, L. Hevesi, C. Van Lint, J. Wouters, Bioorg. Med. Chem. Lett. 19 (2009) 4806–4809.
[25] R. Di Santo, R. Costi, A. Roux, M. Artico, A. Lavecchia, L. Marinelli, E. Novellino, L. Palmisano, M. Andreotti, R. Amici, C.M. Galluzzo, L. Nencioni, A.T. Palamara, Y. Pommier, C. Marchand, J. Med. Chem. 49 (2006) 1939–1945.
[26] R. Di Santo, R. Costi, A. Roux, G. Miele, G.C. Crucitti, A. Iacovo, F. Rosi, A. Lavecchia, L. Marinelli, C. Di Giovanni, E. Novellino, L. Palmisano, M. Andreotti, R. Amici, C.M. Galluzo, L. Nencioni, A.T. Palamara, Y. Pommier, C. Marchand, J. Med. Chem. 51 (2008) 4744–4750.
[27] H. Leh, P. Brodin, J. Bischerour, E. Deprez, P. Tauc, J-C. Brochon, E. Le Cam, D. Coulaud, C. Auclair, J.-F. Mouscadet, Biochemistry 39 (2000) 9285–9294.
[28] X. Wei, J.M. Decker, H. Liu, Z. Zhang, R.B. Arani, J.M. Kilby, M.S. Saag, X. Wu, G.M. Shaw, J.C. Kappes, Antimicrob. Agents Chemother. 46 (2002) 1896–1905.
[29] L. Krishnana, X. Lia, H.L. Naraharisettya, S. Hareb, P. Cherepanov, A. Engelman, Proc. Natl. Acad. Sci. U.S.A. 107 (2010) 15910–15915.
[30] J. Tang, K. Maddali, Y. Pommier, Y.Y. Sham, Z. Wang, Bioorg. Med. Chem. Lett. 20 (2010) 3275–3279.
[31] M. Steiniger-White, I. Rayment, W.S. Reznikoff, Curr.Opin.Struct.Biol. 14 (2004) 50–57.
[32] G. Jones, P. Willett, R.C. Glen, A.R. Leach, R. Taylor, J. Mol. Biol. 267 (1997) 727–748.
[33] E.P. Garvey, B. Schwartz, M.J. Gartland, S. Lang, W. Halsey, G. Sathe, H.L. Carter III, K.L. Weaver, Biochemistry 48 (2009) 1644–1653.
[34] Accelrys Software Inc, Discovery Studio Modeling Environment, Release 2.5. Accelrys Software Inc., San Diego, 2007.
[35] P. Vandurm, C. Cauvin, J. Wouters, E.A. Perpète, D. Jacquemin, Chem. Phys. Lett. 478 (2009) 243–248.